Supporting Information

Local platinum environments in a solid analog of the molecular Periana catalyst

Mario Soorholtz,[a,†,‡] Louis C. Jones,[b,†] Dominik Samuelis,[c] Claudia Weidenthaler,[a] Robin J. White,[d,#] Maria-Magdalena Titirici,[d] David A. Cullen,[e] Tobias Zimmermann,[a] Markus Antonietti,[d] Joachim Maier,[c] Regina Palkovits,[a,f] Bradley F. Chmelka,[b,*] and Ferdi Schüth[a,*]

[a] Max-Plank-Institut für Kohlenforschung, Mülheim an der Ruhr, D-45470, Germany
[b] Department of Chemical Engineering, University of California, Santa Barbara, California 93106-5080, USA
[c] Max Planck Institute for Solid State Research, Stuttgart, D-70569, Germany
[d] Max Planck Institute of Colloids and Interfaces, Potsdam, D-14476, Germany
[e] Oak Ridge National Laboratory, Oak Ridge, Tennessee 37831, USA
[f] RWTH Aachen University, Aachen, D-52074, Germany

Corresponding Author

* bradc@engineering.ucsb.edu

* schueth@mpi-muelheim.mpg.de

Table of Content:

Characterization Details

X-ray absorption spectroscopy (XAS) at the platinum L_3 edge (E_0=11564 eV) was performed at HASYLAB@DESY beamline C. Spectra were recorded *ex situ* in a LN_2 cryostat at 77K in transmission geometry, using ion chambers as detectors (first ion chamber: 150 mbar Kr; second and third ion chamber: 900 mbar Kr). Energy range was [11364;12164] eV, with ΔE=10 eV steps in the pre-edge range to 11534 eV, ΔE=1 eV steps up to 11554 eV, ΔE=0.5 eV steps to 11574 eV (covering the edge step), ΔE=1 eV steps to 11574 eV, and finally *k*-space equidistant scanning with Δk=0.025 between 11574 and 12164 eV. Sampling time was 1 second for each data point in constant-ΔE scanning and from 1 to 4 seconds for constant-Δk scanning. A platinum foil reference for energy calibration, placed between second and third ion chamber, was measured simultaneously. In order to avoid higher harmonics passing the Si(111) double crystal monochromator, the second crystal was detuned to 50% of the maximum intensity, using the D-Mostab monochromator stabilization system.[1, 2] Sample pellets for transmission measurements were prepared by homogenizing between 15 and 30 mg of the finely ground catalyst sample with approx. 40 mg binder/diluent, consisting of (80:20) cellulose (Aldrich) and graphite powder (Aldrich) for improved heat conduction, followed by uniaxial pressing at 30 kN for 60 s, and yielding a self-supporting pellet with d=12 mm. Three to four spectra were recorded per sample. After checking for reproducibility, spectra were aligned in E-space and energy-calibrated *via* the Pt reference foil spectra. EXAFS spectra were extracted from the merged data according to the standard procedures, using the IFEFFIT/HORAE[3, 4] software suite and the AutoBK[5] algorithm. The geometrical model for the EXAFS refinement was based on coordinates of the

analogous homogeneous catalyst Pt(bpym)Cl_2, obtained from DFT-based geometry optimization.

High resolution high-angle annular dark-field (HAADF) STEM images were recorded using a JEOL 2200FS operated at 200 kV and equipped with a CEOS GmbH hexapole aberration corrector, which provides a sub-Angstrom electron probe for imaging and spectroscopic analysis. Powders were sonicated in methanol and then evaporatively dispersed on the TEM grids.

Solid-state ^{195}Pt WURST-CPMG NMR spectra were acquired at 7.06 T on a Bruker AVANCE NMR spectrometer operating at 300.07 and 64.49 MHz for ^{1}H and ^{195}Pt, respectively, with parameters optimized according to references.[6, 7] WURST-CPMG pulses of 50 μs (~2 MHz) were applied at center frequencies of 64.72 and 64.28 MHz using forward and reverse frequency sweeps to compensate for transverse relaxation of ^{195}Pt magnetization during the sweeps. An acquisition time of 80 μs was used to measure the free induction decays of each subsequent CPMG loop (12 total) with recycle delays of 0.5 to 2 s, which were chosen to maximize signal sensitivity. Fourier transformed spectra for the two center frequencies were co-added after a magnitude calculation to produce the observed ^{195}Pt spikelet patterns with a span of >1 MHz. Lineshape analyses were performed using the program *dmfit* based on interpolated skyline projections of each characteristic CPMG spikelet pattern.[8] ^{195}Pt chemical shifts are referenced with respect to 1.0 M Na_2PtCl_6 (aq) (δ_{iso}=0.0 ppm).

Nitrogen sorption measurement was carried out at 77 K on a Micrometrics ASAP 2010 instrument. Samples were activated under vacuum for at least 15 h at 150 °C. Pore size distribution, pore volume and surface area were calculated using Autosorb software

(version 1.52) using the NLDFT equilibrium model (N_2 at 77K on carbon (slit/cylindrical pore model). Comparison of calculated NLDFT and measured sorption data exhibit a match of > 97%.

XRD patterns were collected with a Bragg Brentano diffractometer (STOE THETA/THETA). The instrument was equipped with a secondary graphite monochromator (Cu$K_{\alpha 1,2}$ radiation) and a proportional gas detector. The divergence slit was set to 0.8°, the receiving slit was set to 0.8 mm, and the width of the horizontal mask was 4 mm. The samples were prepared on a background free single crystal quartz sample holder.

Thermogravimetry experiments were performed using a Netzsch STA 449C thermal analyzer applying a heating rate of 10°C min^{-1} in a flow of air (60 mL min^{-1}).

FT-IR spectra were recorded on a Magna System 560 equipped with a Ge-ATR-crystal. Each sample was scanned 128 times with a resolution of 2 cm^{-1}.

XPS (X-ray photoelectron spectroscopy) measurements were performed with a Kratos HSi spectrometer with a hemispherical analyzer. The monochromatized Al K_α X-ray source (E=1486.6 eV) was operated at 15 kV and 15 mA. For the narrow scans, an analyzer pass energy of 40 eV was applied. The hybrid mode was used as lens mode. The base pressure during the experiment in the analysis chamber was 4 x 10^{-7} Pa. To consider surface charging effects of carbonized samples, the binding energy values were referenced to the graphitic C 1s carbon peak at 284.5 eV. CTF materials were measured as pressed pellets with a fraction of (nitrogen free) cellulose (mass ratio: CTF/cellulose = ~3) in order to fix the sample within the XPS chamber. Accuracy of given binding energies is in the range of ±0.2 eV.

Scanning electron microscopy (SEM) micrographs were collected on a Hitachi S-5500 ultra-high resolution cold field emission scanning electron microscope. The instrument was operated at a maximum acceleration voltage of 30 kV.The samples were embedded in Spurr resin (hard-mixture) in a two-step procedure. After trimming the tip to around 150μm², a Diamond-knife in an Ultramicrotom (Reichert Ultracut) was used for sectioning. The thickness of the sections is around 30 nm.

The ^{13}C CP-MAS NMR spectrum was recorded on a Bruker Avance 500WB spectrometer at a resonance frequency of 125.8 MHz using a double-bearing MAS probe (DVT BL4). The experimental conditions were as follows: 12 kHz spinning rate, 2 s recycle delay, 27,300 scans, 1 ms contact time, and 4.3 μs ^{1}H $\pi/2$ pulse. The chemical shift was referenced to neat TMS in a separate rotor.

TEM micrographs of Figure S9 were obtained on an HF-2000 instrument. The HF-2000 instrument is equipped with a cold field emitter (CFE) and can be operated at a maximum acceleration voltage of 200 kV. Typically the samples were placed on a Lacey carbon film supported by a copper grid. Solid samples were deposited on the Lacey carbon film without previous dissolution.

Experimental Details

Covalent Triazine Framework (CTF) was synthesized according to the method of Kuhn *et al.*[9]. Zinc chloride and 2,6-dicyanopyridine were stored in a glove box after intensive drying in high vacuum (10^{-3} mbar) at 150°C for 30°C, respectively. 3.362 g (0.025 mol) $ZnCl_2$ and 0.646 g (0.005 mol) 2,6-dicyanopyridine were thoroughly mixed and filled into a quartz ampule (12 x 1 cm). This ampule was evacuated, sealed and placed into an ampule oven with no temperature gradients. The sample was thermally treated at 400°C with a heating rate of 15°C min^{-1} and a hold time of 40 h in a first sequence. In a second sequence, the sample was treated at 600°C with a heating ramp of 10°C min^{-1} and a hold time of 40 h before the sample was cooled down to room temperature. After opening the quartz ampule, the monolithic material was intensively washed with water and hydrochloric acid. Finally, the sample was dried in a vacuum oven at 50°C.

Dichlorobipyrimidyl platinum(II) ($Pt(bpym)Cl_2$) was synthesized as described according to the method of Kiernan *et al*[10]. For the coordination of platinum to the solid material, analogous to the method of P. M. Kiernan *et al.*[10] and Ziatdinov[11], 400 mg of the carbon was added to 1 L water that contained 46 mg of dissolved K_2PtCl_4. The mixture was stirred for 24 h at room temperature. After filtration, the solid was intensively washed with water to remove non-coordinated Pt species.

References

(1) Krolzig, A.; Materlik, G.; Swars, M.; Zegenhagen, J. *Nucl. Instr.Meth. Phys. Res.* **1984**, *219*, 430-434.

(2) Meß, K.; Tröger, L.; Brüggemann, U. In *HASYLAB Annual Report 1998*, Laasch, W., Materlik, G., Schneider, J. R., Schulte-Schrepping, H., Eds.; Hamburger Synchrotonstrahlungslabor HASYLAB, Hamburg, Germany, 1998.

(3) Ravel, B.; Newville, M. *J. Synchrotron Radiat.* **2005**, *12*, 537-541.

(4) Newville, M. *J. Synchrotron Radiat.* **2001**, *8*, 322-324.

(5) Newville, M.; Līviņš, P.; Yacoby, Y.; Rehr, J. J.; Stern, E. A. *Phys. Rev. B* **1993**, *47*, 14126-14131.

(6) O'Dell, L. A.; Schurko, R. W. *Chem. Phys. Lett.* **2008**, *464*, 97-102.

(7) MacGregor, A. W.; O'Dell, L. A.; Schurko, R. W. *J. Magn. Reson.* **2011**, *208*, 103-113.

(8) Massiot, D.; Fayon, F.; Capron, M.; King, I.; Le Calvé, S.; Alonso, B.; Durand, J.-O.; Bujoli, B.; Gan, Z.; Hoatson, G. *Magn. Reson. Chem.* **2002**, *40*, 70-76.

(9) Kuhn, P.; Thomas, A.; Antonietti, M. *Macromolecules* **2009**, *42*, 319-326.

(10) Kiernan, P. M.; Ludi, A. *Dalton Trans.* **1978**, 1127-1130.

(11) Ziatdinov, V. R. Dissertation, University of Southern California, 2007.

(12) Xu, X.; Kua, J.; Periana, R. A.; Goddard, W. A. *Organometallics* **2003**, *22*, 2057-2068.

Supplementary Results

X-ray diffraction (XRD):

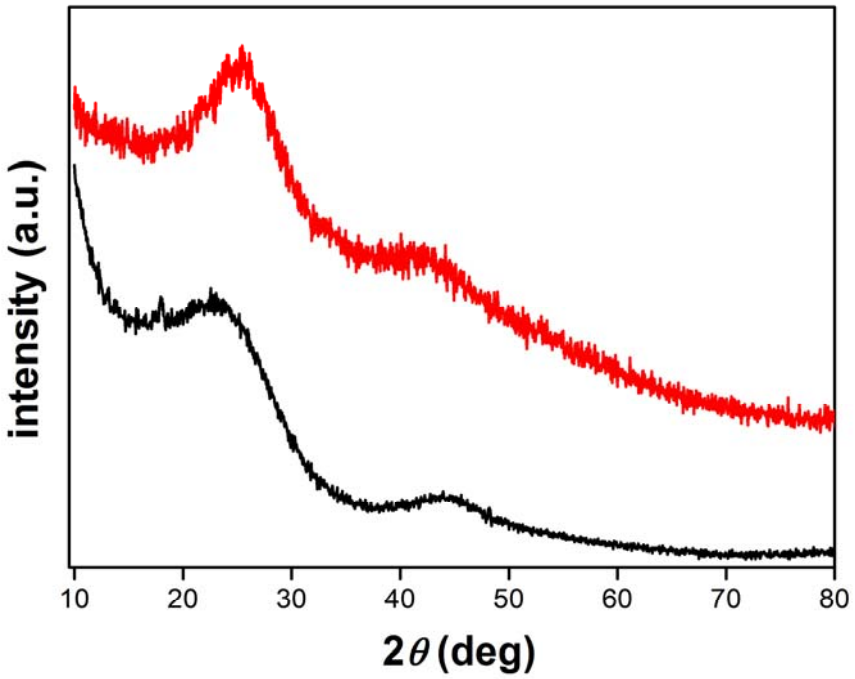

Figure S1. Powder XRD patterns of non-modified CTF (black) and Pt-modified CTF (red). Both XRD patterns exhibit characteristics for carbon materials with aromatic stacking. Moreover, no reflections for metallic platinum can be observed for Pt-modified CTF. Minor differences in lineshape can be attributed to different particle sizes between CTF and Pt-CTF.

Solid-State ^{195}Pt NMR

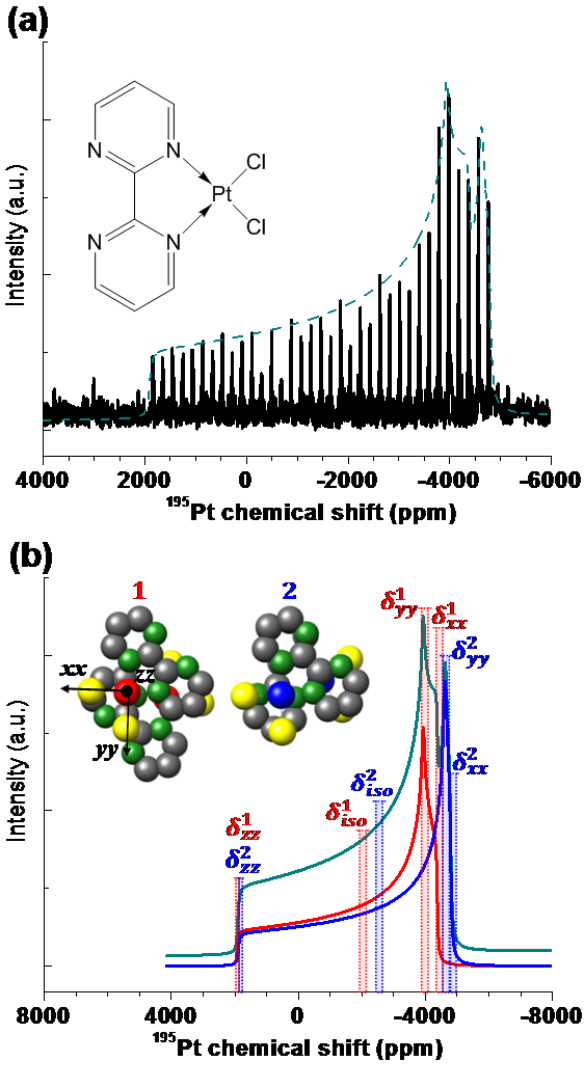

Figure S2. (a) Static solid-state ^{195}Pt WURST-CPMG NMR spectrum (black) and summed fit (dashed green) of **(b)** lineshapes that correspond to the two distinct equally populated ^{195}Pt atom sites in crystalline (bpym)$PtCl_2$. Proposed local structures of the ^{195}Pt sites (1, red; 2, blue) are shown as insets above each spectrum, with nitrogen atoms (green), carbon atoms (grey), and chlorine atoms (yellow). Chemical shift parameters (δ_{xx}, δ_{yy}, δ_{zz}, and δ_{iso}) are descriptors of the local ^{195}Pt bonding environments and are indicated for each lineshape, specific values of which are tabulated in Table S3. Axes shown for site 1 indicate the orthogonal coordinate system of the site's ^{195}Pt chemical shift tensor.

Table S1. ^{195}Pt chemical shift parameters for as-synthesized Pt-CTF catalyst

Chemical Shift Tensor Parameters [ppm]				Chemical Shift Anisotropy Parameters			
Component	δ_{xx}	δ_{yy}	δ_{zz}	δ_{iso} [ppm]	$\Delta\sigma/\Delta\delta$ [ppm]	η	% Area
I	-4900 +/- 200	-4500 +/- 200	6400 +/- 200	-1000 +/- 200	7400 +/- 400	0.06 +/- 0.04	75 +/- 10
II	NA	NA	NA	-4200 +/- 200	1500 +/- 400	NA	25 +/- 10

Table S2. ^{195}Pt chemical shift parameters for used Pt-CTF catalyst after reaction.

Chemical Shift Tensor Parameters [ppm]				Chemical Shift Anisotropy Parameters			
Component	δ_{xx}	δ_{yy}	δ_{zz}	δ_{iso} [ppm]	$\Delta\sigma/\Delta\delta$ [ppm]	η	% Area
I	-4900 +/- 200	-4500 +/- 200	6400 +/- 4500	-1000 +/- 1500	7400 +/- 400	0.06 +/- 0.04	53 +/- 10
II	NA	NA	NA	-4200 +/- 200	1500 +/- 400	NA	47 +/- 10

Table S3. ^{195}Pt chemical shift parameters for polycrystalline Pt(bpym)Cl_2.

Chemical Shift Tensor Parameters [ppm]				Chemical Shift Anisotropy Parameters			
Component	δ_{xx}	δ_{yy}	δ_{zz}	δ_{iso} [ppm]	$\Delta\sigma$ [ppm]	η	% Area
1	-4400 +/- 200	-3900 +/- 200	1900 +/- 200	-2100 +/- 200	4100 +/- 400	0.11 +/- 0.04	50 +/- 5
2	-4800 +/- 200	-4600 +/- 200	1900 +/- 200	-2500 +/- 200	4400 +/- 400	0.04 +/- 0.04	50 +/- 5

Catalyst recycling

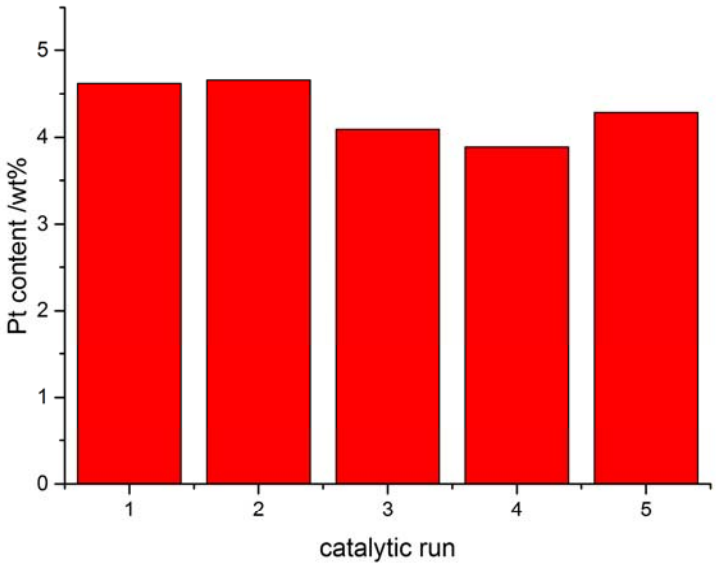

Figure S3. Platinum content of Pt-CTF in recycling experiments. Pt-CTF (~5 wt% Pt) was tested in 5 subsequent catalytic runs (reaction conditions: 215°C, 2.5 h, 15 mL oleum (20 wt.% SO_3), 90 bar CH_4) and analyzed for its platinum content. After each run the catalyst was filtered off at room temperature from the reaction solution and thoroughly washed with water and acetone. After drying an aliquot was analyzed for its platinum content (atomic absorption spectroscopy, AAS, Mikroanalytisches Laboratorium Kolbe, Mülheim) and the residual catalyst used in the next experimental run. These experiments indicate a stable platinum loading of ~4-5 wt% for the Pt-CTF material used under these conditions over five subsequent experiments.

Table S4. Platinum contents of Pt-CTFs before and after catalysis measured with various techniques.

measurement	*platinum content before /wt%*	*platinum content after /wt%*
AAS	15.0	6.7
XAS	27.5 ±13.3	4.1 ±2.0
XPS	18.2	n.a.
SEM-EDX	15.0	n.a.

Samples before catalysis were measured with high metal contents in favor of a high S/N ratio. Samples after catalysis showed a lower S/N ratio consistent with partial leaching of platinum.

X-Ray Absorption Spectroscopy (XAS)

Table S5. Mass fraction of platinum within Pt-CTF samples. Metal concentrations were determined by dividing the edge step Δμ by catalyst mass present in pellets (assuming homogeneous distribution of platinum throughout the sample pellet, identical diameter of all pellets, and constant X-ray beam size). High error limits were obtained due to the low transition metal content of investigated sample pellets and, thus, due to high signal/noise ratio.

sample	$mass_{platinum}$ *[wt.%]*	*limit of error [wt.%]*
Pt-CTF-(sample 1)	27.5	± 13.3
Pt-CTF-(sample 2)	22.1	± 10.7
Pt-CTF-(sample 3)	17.9	± 8.7
Pt-CTF-(sample 4)	7.9	± 3.8
Pt-CTF-(sample 1)‡	4.1	± 2.0

‡= sample tested under reaction conditions prior to XAS measurement (reaction conditions: 215°C, 2.5 h, 15 mL oleum (20 wt.% SO3), 90 bar CH4).

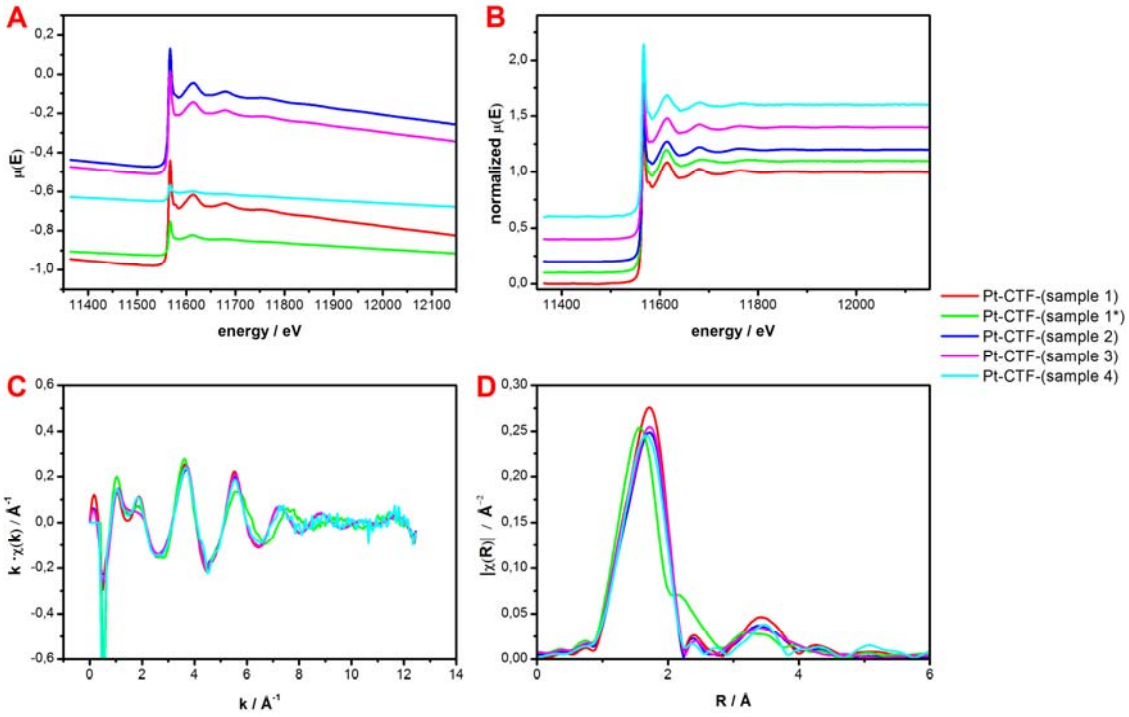

Figure S4. X-ray absorption spectroscopy data. * = sample tested under reaction conditions prior to XAS measurement (reaction conditions: 215°C, 2.5 h, 15 mL oleum (20 wt.% SO_3), 90 bar CH_4); (A) μ(E) raw data; (B) normalized μ(E) data (offsets were introduced in order to visually differentiate samples); (C) χ(*k*)·*k* functions; (D) Fourier-transformed χ(*k*)·*k* functions for investigated Pt-CTF samples. As mentioned above, a first-shell EXAFS fit was complicated by the fact that the expected Pt-N distance (2.05 Å) is similar to the

(non-bonding) Pt-C distance (2.89 Å) for the two carbon atoms bridging the pyrimidine rings, and also from the distance to the next-nearest Pt-C (3.05 Å). In addition, there are two more ligands bound to the Pt, and their distances from the Pt center are approximately 2.4 Å. All of this leads to a very broad first shell signal in the EXAFS spectra; isolation and speciation of the overlapping individual contributions by fitting the EXAFS has to be based on a number of constraints to interpret the information content of the spectra. EXAFS fitting was applied to one Pt-CTF sample that was used in the direct oxidation of methane in sulfuric acid and a series of as-prepared Pt-CTF materials. Fits were done with multiple k-weights, *i.e.* k=1 and k=2 simultaneously. As shown, we were able to fit all pre-catalysis EXAFS spectra with identical structural models, assuming the first coordination shell to contain the (bpym) ligand and 2 Cl^- ligands, and assuming a mirror plane along the Pt – (midpoint C5/C6) axis and perpendicular to the C5/C6 bond (see Fig. 2A), with very high fit quality. Multiple scattering paths had to be included to account for the significant intensity in the region of 3 Å < R_{EXAFS} < 4 Å.

Table S6. Statistical data and amplitude factor S_0^2 of fitted EXAFS functions.

sample	*R factor*	S_0^2	*limit of error for* S_0^2
Pt-CTF-(sample 1)	0.0226	0.8775	± 0.1114
Pt-CTF-(sample 2)	0.0260	0.8350	± 0.1286
Pt-CTF-(sample 3)	0.0193	0.7925	± 0.0882
Pt-CTF-(sample 4)	0.0214	0.8296	± 0.0963
Pt-CTF-(sample 1)*†	0.0369	0.8394	± 0.1317
Pt-CTF-(sample 1)*‡	0.0246	0.9231	± 0.2061

*= sample tested under reaction conditions prior to XAS measurement (reaction conditions: 215°C, 2.5 h, 15 mL oleum (20 wt.% SO3), 90 bar CH4). †Pt(bipym)Cl(HSO_4) model ‡Pt(bpym)Cl_2 model

Table S7a. Geometric parameters of fitted EXAFS functions. Bond descriptions can be taken from Figure 2A. (* = values were derived from structural model taken from Xu *et al.*[12])

sample	*distance Pt-N1 [Å]*	*±[Å]*	*distance Pt-Cl [Å]*	*±[Å]*	*distance Pt-C4 [Å]*	*±[Å]*	*distance Pt-C1 [Å]*	*±[Å]*
$Pt(bpym)Cl_2$*	2.047	0.000	2.375	0.000	2.895	0.000	3.054	0.000
Pt-CTF-(sample 1)	1.965	0.055	2.258	0.046	2.759	0.051	2.912	0.052
Pt-CTF-(sample 2)	1.967	0.053	2.260	0.045	2.763	0.050	2.916	0.052
Pt-CTF-(sample 3)	1.949	0.064	2.248	0.054	2.757	0.059	2.912	0.061
Pt-CTF-(sample 4)	1.965	0.050	2.259	0.043	2.760	0.048	2.913	0.049
Pt-CTF-(sample 1)‡	1.947		2.161		2.656		2.808	

‡ sample used in the selective oxidation of methane; distances are considerable different indicating the invalidity of the $Pt(bpym)Cl_2$ model for this sample

Table S7b. Geometric parameters of fitted EXAFS functions. Bond descriptions can be taken from Figure 2A. (* = values were derived from structural model taken from Xu *et al.* [12])

sample	*distance Pt-N2 [Å]*	*± [Å]*	*distance Pt-C2 [Å]*	*±[Å]*	*distance Pt-C3 [Å]*	*±[Å]*
$Pt(bpym)Cl_2$*	4.183	0.000	4.333	0.000	4.747	0.000
Pt-CTF-(sample 1)	4.027	0.076	4.147	0.065	4.547	0.069
Pt-CTF-(sample 2)	4.033	0.074	4.154	0.065	4.554	0.069
Pt-CTF-(sample 3)	4.043	0.088	4.166	0.076	4.571	0.080
Pt-CTF-(sample 4)	4.027	0.070	4.148	0.061	4.548	0.065
Pt-CTF-(sample 1)‡	3.986		4.029		4.424	

Table S8. Variance σ^2 of various scattering pathways. Bond descriptions can be taken from Figure 2A.

sample	*Pt-N1*	±	*Pt-Cl*	±	*Pt-C1 and Pt-C4*	±	*Pt-N2*	±
$Pt(bpym)Cl_2$	-	-	-	-	-	-	-	-
Pt-CTF-(sample 1)	-0.0007	0.0027	0.0009	0.0019	0.0307	0.0165	-0.0015	0.0065
Pt-CTF-(sample 2)	-0.0006	0.0023	0.0006	0.0016	0.0369	0.0192	-0.0010	0.0059
Pt-CTF-(sample 3)	-0.0004	0.0030	0.0030	0.0026	0.0366	0.0232	3.6885	3566959
Pt-CTF-(sample 4)	-0.0009	0.0022	0.0005	0.0016	0.0354	0.0173	-0.0017	0.0053
Pt-CTF-(sample 1)‡	0.0023	0.0035	0.0086	0.0049	0.0039	0.0072	0.1049	0.4627

‡sample used in the selective oxidation of methane; l

Table S9. First shell coordination numbers for Pt-CTF after use in catalysis. First shell content as refined from EXAFS fits with a model comprising Pt-N, Pt-Cl contributions from the $Pt(bpym)Cl_2$ and Pt-O contributions from OSO_3H ligand. Standard reaction conditions: 2.5h (215°C, 15 mL oleum (20 wt.% SO_3), 90 bar CH_4).

sample	*coordination number for*				
	N	±	*O*	±	*Cl*
Pt-CTF-(sample1)‡	1.94494	0.53540	1.06574	0.3746	0.98932
Pt-CTF-(sample 2)‡	1.48766	0.55540	1.20588	0.48115	1.30640
Pt-CTF-(sample 3)‡	1,80882	0,46070	1,08121	0,35302	1,10997
Pt-CTF-(sample 4)‡	2,06225	0,56203	1,00658	0,33698	0,93116

Electron microscopy

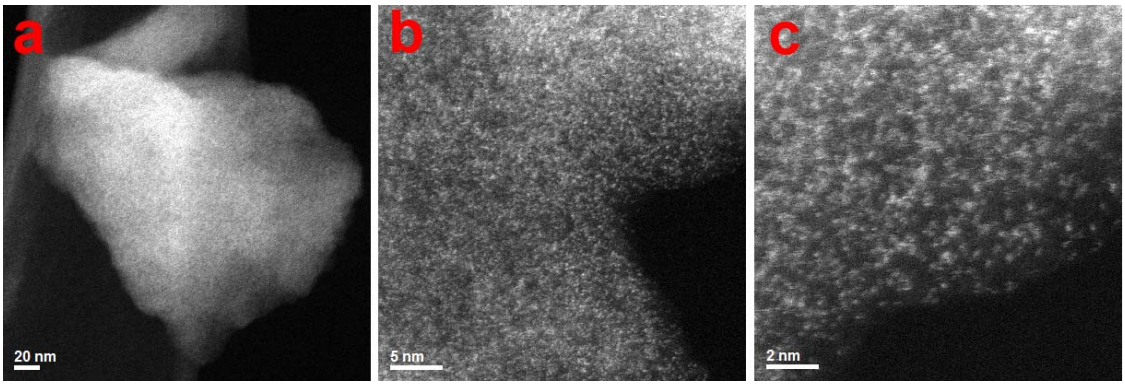

Figure S5. Electron microscopy analysis of Pt-CTF. AC-HAADF-STEM images of Pt-CTF material before use in catalysis clearly show the presence of atomic Pt species. Atomic dispersion was best demonstrated at the thin edges of the CTF particles, where overlap and thickness effects could be avoided.

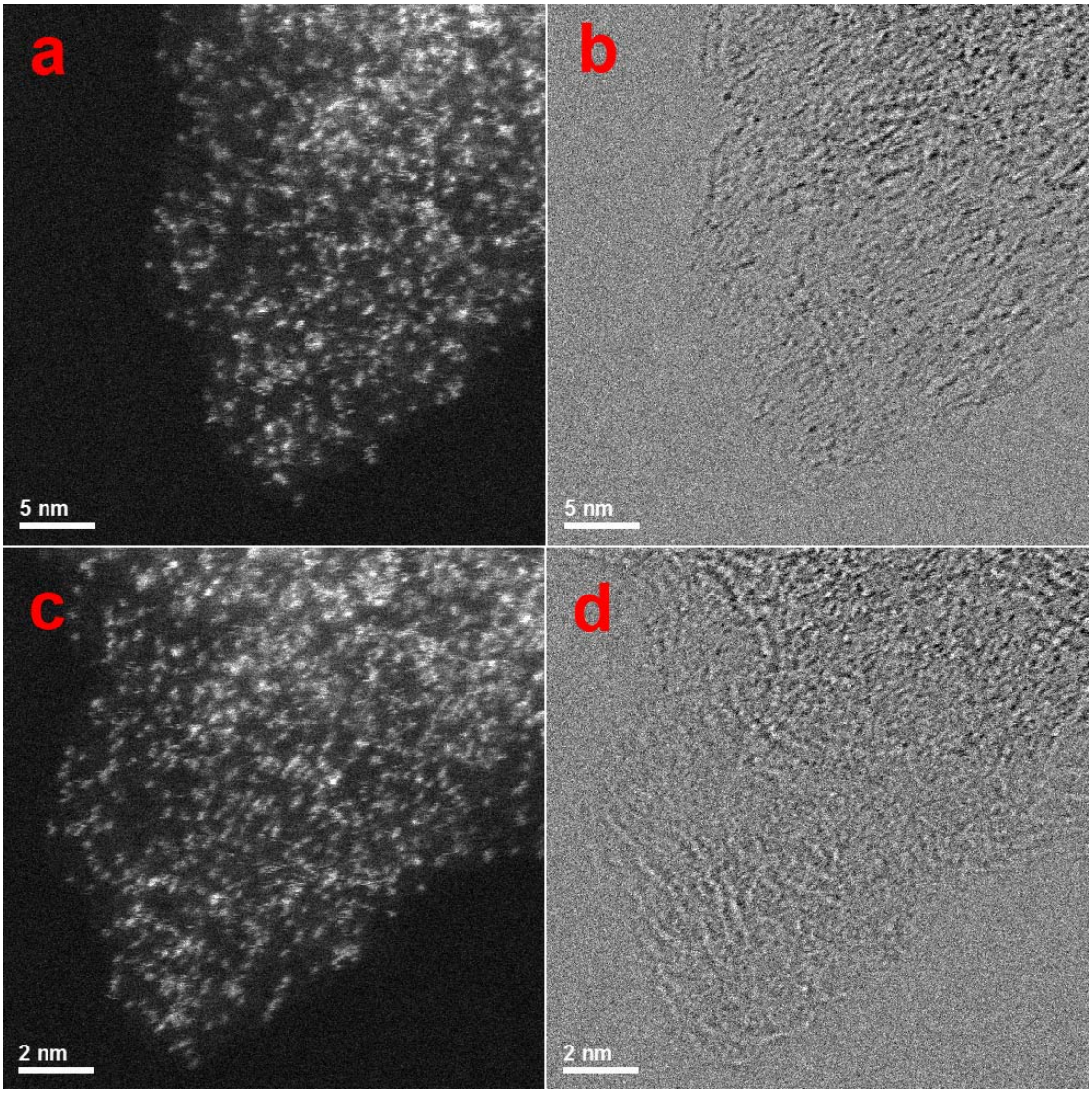

Figure S6. Electron microscopy analysis of Pt-CTF after catalysis. HAADF (**a+c**) and bright-field (**b+d**) STEM images of respective identical locations of Pt-CTF material after several catalytic runs clearly shows that the homogeneous dispersion of single Pt atoms is maintained.

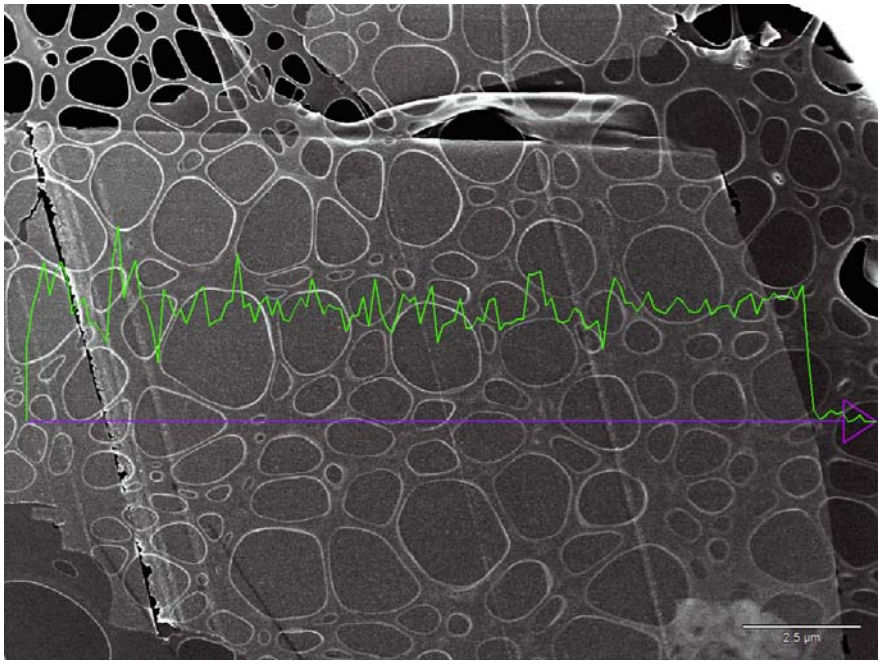

Figure S7. EDX analysis of Pt-CTF. SEM image of a cross-section cut of Pt-CTF with a thickness of around 30 nm. Green line indicates EDX signal referring to Pt, purple arrow demonstrates position of electron beam during analysis.

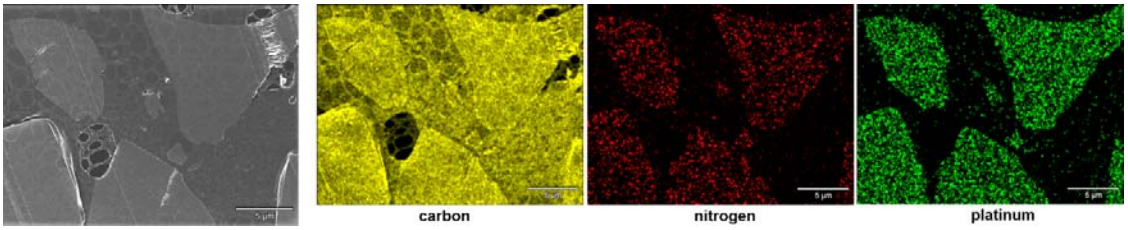

Figure S8. EDX analysis of Pt-CTF. SEM image of Pt-CTF cross-section cuts and the corresponding EDX mapping for carbon, nitrogen and platinum. A homogeneous distribution of Pt within the CTF particles can be observed. In the case of EDX mapping of carbon, species between cuts can be found since Pt-CTF particles are embedded in a carbon-based polymer during sample preparation.

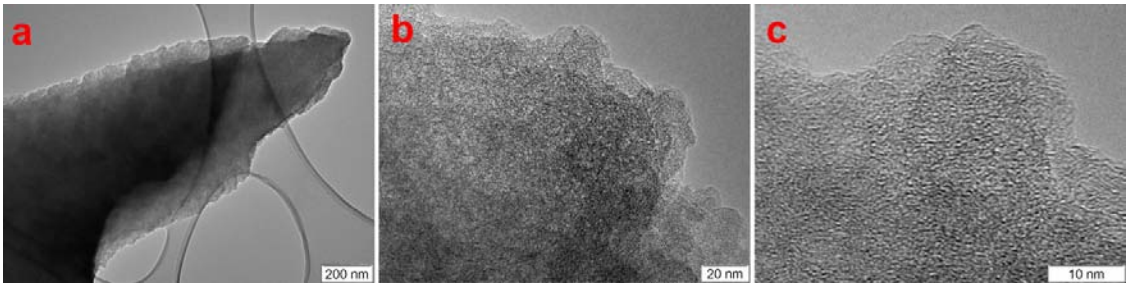

Figure S9. Electron microscopy analysis of CTF. TEM images (**a-c**) illustrate CTF morphology of a representative carbon particle.

Nitrogen sorption

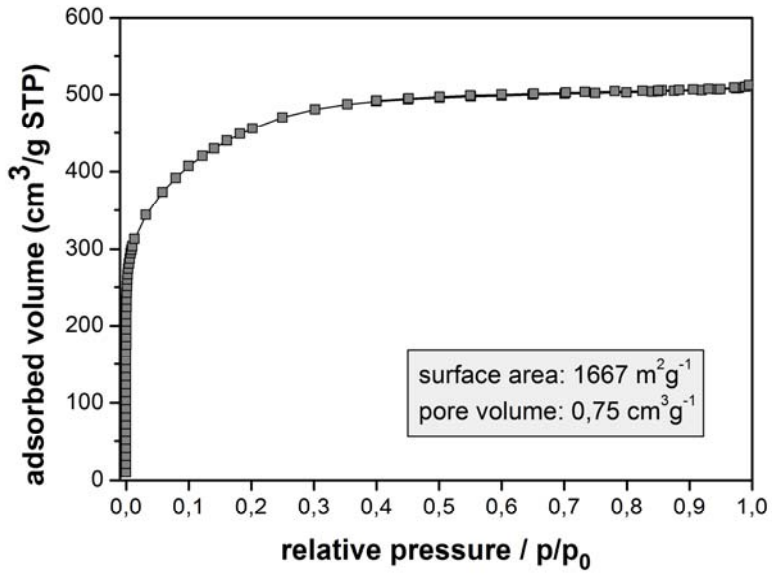

Figure S10. N_2 sorption isotherm of CTF. N_2 sorption for non-modified CTF material based on 2,6-dicyanopyridine as monomer exhibits a Type I-like isotherm. Specific surface area and pore volume of CTF were calculated from NLDFT equilibrium model (see inset).

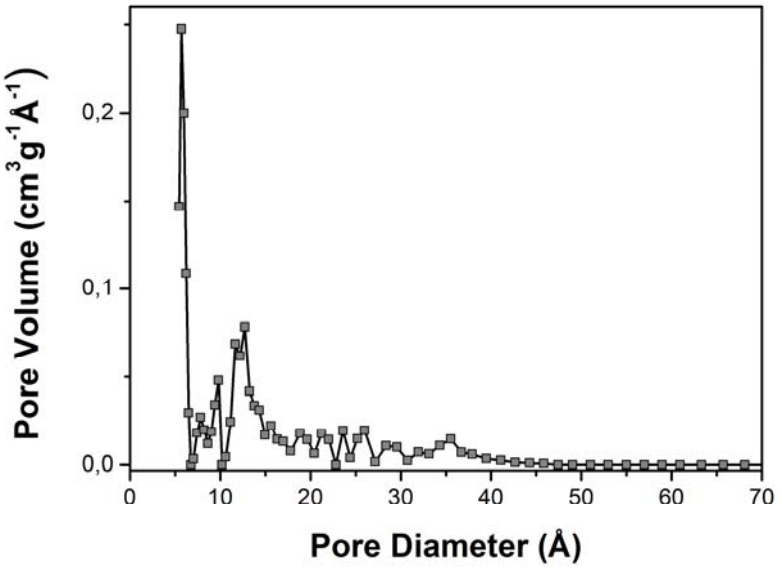

Figure S11. NLDFT pore size distribution for non-modified CTF material. Calculated pore size distribution for CTF material clearly shows its microporous character, however, a relatively small fraction of mesopores with a pore size > 2 nm are present as well.

Thermogravimetry (TG):

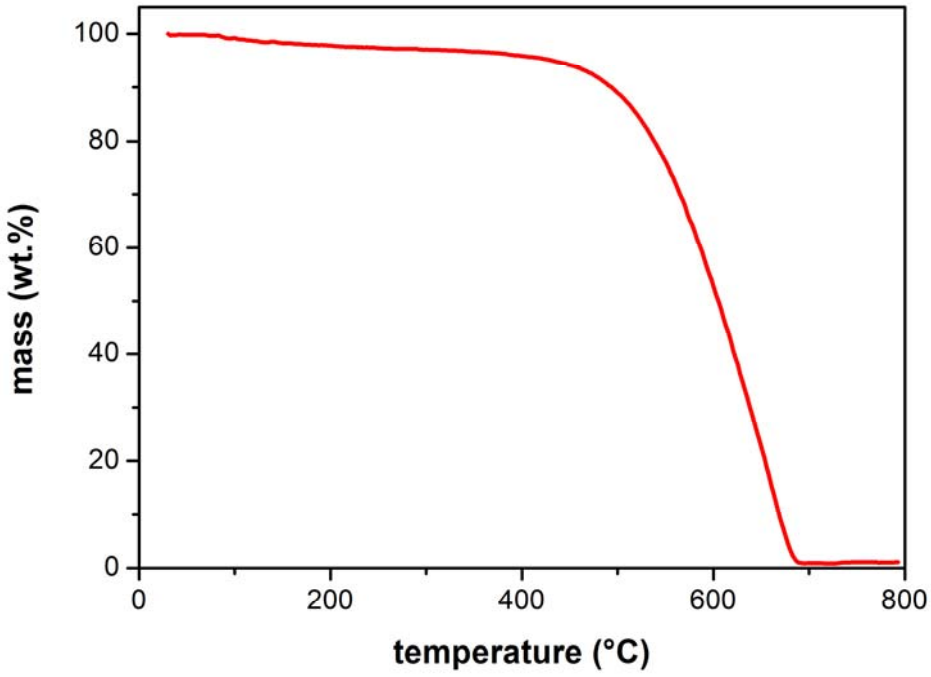

Figure S12. Thermogravimetry profile of CTF in air. Thermogravimetry investigation of CTF material in a flow of air (60 mL min^{-1}) with a heating rate of 10°C min^{-1} indicates good thermal stability of the carbon framework. In detail, significant weight loss can only be observed at temperatures > 400°C, which can be attributed to the oxidation of the carbon scaffold and the formation of CO_2.

X-ray photoelectron spectroscopy (XPS)

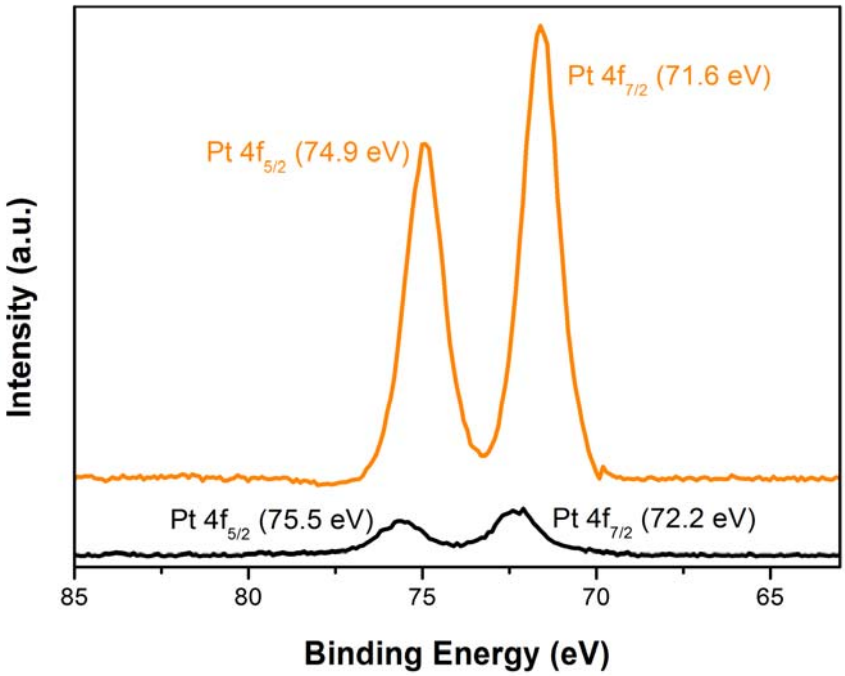

Figure S13. XPS Pt *4f* spectra for Pt-CTF and Pt(bpym)Cl_2. Accurate comparison of Pt 4f binding energies for Pt(bpym)Cl_2 (orange) and Pt-CTF (black) is challenging since determination of a common C 1s reference peak is hardly possible. The graphitic C 1s peak is normally used as reference peak for the investigation of carbon materials (see *Characterization Details*). However, since graphitic carbon is not present in the structure of 2,2'-bipyrimidine and both materials do not share a common defined C 1s peak an accurate comparison is not feasible and, thus, the interpretation of relative peak positions is difficult. Different intensities in Pt 4f spectra are attributed to different weight fractions of platinum in Pt-CTF and Pt(bpym)Cl_2, respectively.

FT-IR Spectroscopy: Attenuated Total Reflectance (ATR)

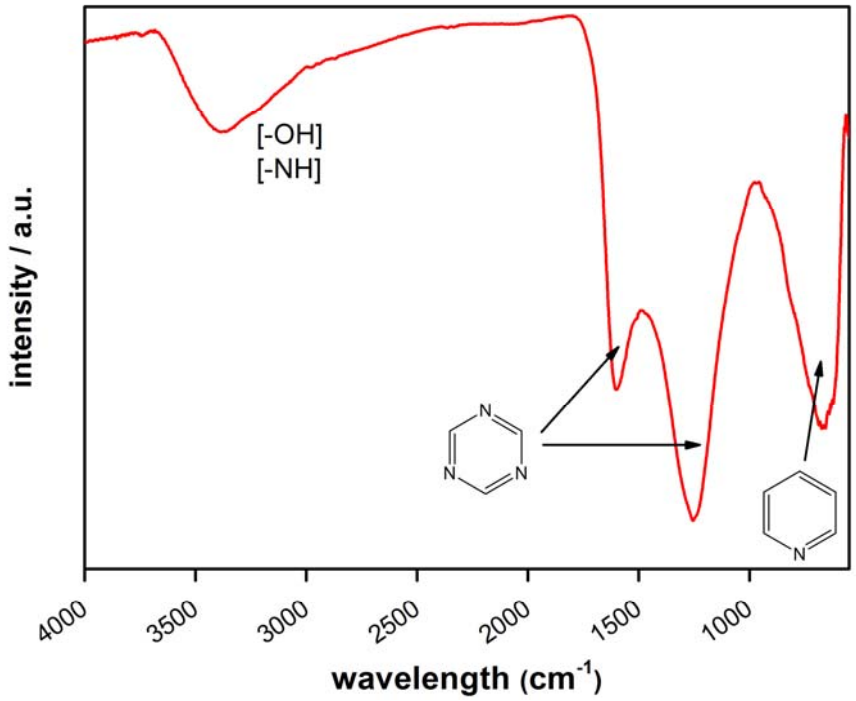

Figure S14. Fourier transform infrared (FT-IR) spectrum of CTF material. The FT-IR spectrum of CTF exhibits characteristic peaks for the expected triazine and pyridine functionalities. However, the broad peak between 3750-2750 cm^{-1} represents (-NH), (-OH) or (-COOH) functionalities, which can possibly be attributed to the acidic hydrolysis of terminal nitrile groups of the CTF scaffold in the course of CTF synthesis procedure.

Solid-state ^{13}C CP-MAS NMR

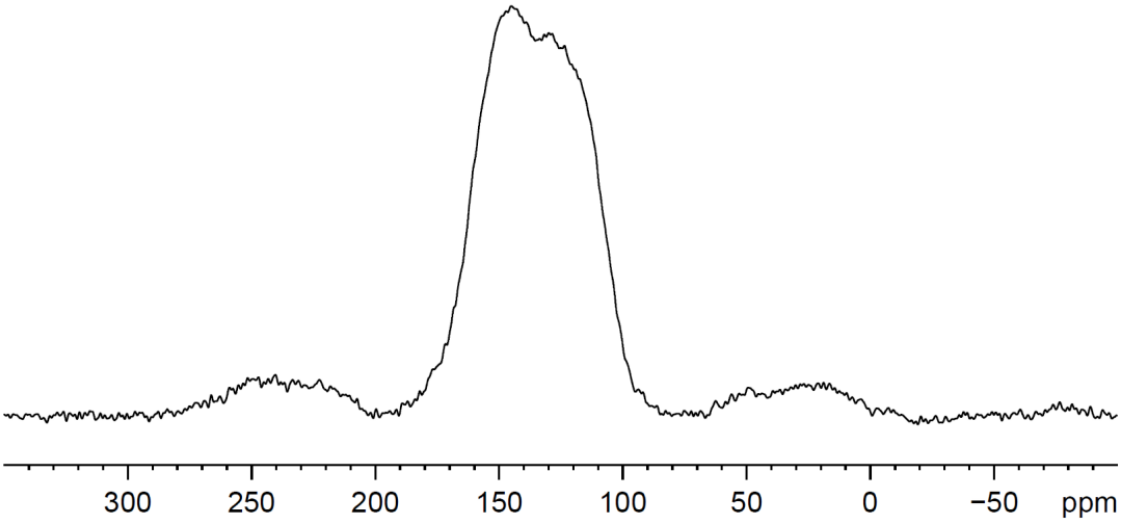

Figure S15. Solid-state ^{13}C NMR analysis of Pt-CTF. The ^{13}C CP-MAS NMR spectrum for Pt-CTF exhibits a broad peak in the range of 100-180 ppm indicating a broad range of carbon species which can be attributed to the high polymerization temperatures of up to 600°C and, thus, to a mild carbonization process leading to the rearrangement of the carbon scaffold. Similar behavior could be observed from the XPS N1s spectra of CTF indicating the presence of additional nitrogen species (other than pyridine nitrogen) which result from thermally induced rearrangement of the CTF network. However, the strong resonances in the range of δ = 90-160 ppm suggest the exclusive presence of aromatic carbon species.